Controlling charge and current neutralization of an ion beam pulse in a background plasma by application of a solenoidal magnetic field: Weak magnetic field limit

I. D. Kaganovich, E. A. Startsev, A. B. Sefkow, and R. C. Davidson
Princeton Plasma Physics Laboratory, Princeton, New Jersey 08543, USA

(Received 22 February 2008; accepted 23 September 2008; published online 27 October 2008)

Propagation of an intense charged particle beam pulse through a background plasma is a common problem in astrophysics and plasma applications. The plasma can effectively neutralize the charge and current of the beam pulse, and thus provides a convenient medium for beam transport. The application of a small solenoidal magnetic field can drastically change the self-magnetic and self-electric fields of the beam pulse, thus allowing effective control of the beam transport through the background plasma. An analytic model is developed to describe the self-magnetic field of a finite-length ion beam pulse propagating in a cold background plasma in a solenoidal magnetic field. The analytic studies show that the solenoidal magnetic field starts to influence the self-electric and self-magnetic fields when $\omega_{ce} \gtrsim \omega_{pe}\beta_b$, where $\omega_{ce}=eB/m_e c$ is the electron gyrofrequency, ω_{pe} is the electron plasma frequency, and $\beta_b=V_b/c$ is the ion beam velocity relative to the speed of light. This condition typically holds for relatively small magnetic fields (about 100 G). Analytical formulas are derived for the effective radial force acting on the beam ions, which can be used to minimize beam pinching. The results of analytic theory have been verified by comparison with the simulation results obtained from two particle-in-cell codes, which show good agreement. © *2008 American Institute of Physics*. [DOI: 10.1063/1.3000131]

I. INTRODUCTION

Background plasma can be used as an effective neutralization scheme to transport and compress intense charged particle beam pulses. To neutralize the large repulsive space-charge force of the beam particles, the beam pulses can be transported through a background plasma. The plasma electrons can effectively neutralize the beam charge, and the background plasma can provide an ideal medium for beam transport and focusing. Neutralization of the beam charge and current by a background plasma is an important issue for many applications involving the transport of fast particles in plasmas, including astrophysics,[1–4] accelerators,[4,5] and inertial fusion, in particular, fast ignition[6] and heavy ion fusion,[7,8] magnetic fusion based on field reversed configurations fueled by energetic ion beams,[9] the physics of solar flares,[10] as well as basic plasma physics phenomena.[11]

Previous studies have explored the option of ion beam pulse neutralization by passing the beam pulse through a layer of plasma or a plasma plug.[12] The ion beam pulse extracts electrons from the plasma plug and drags electrons along during its motion outside the plasma plug region. There are several limitations of this scheme. When the intense ion beam pulse enters the plasma, the electrons stream into the beam pulse in the strong self-electric and self-magnetic fields, attempting to drastically reduce the ion beam space charge from a non-neutralized state to a completely neutralized state. After the ion beam pulse exits the plasma, the beam carries along the electrons, with average electron density and velocity equal to the ion beam's average density and velocity. However, large-amplitude plasma waves are excited in a nonstationary periodic pattern resembling butterfly wing motion.[13] Due to these transient effects, the beam may undergo transverse emittance growth, which would increase the focal spot size.[14] Smoother edges to the plasma plug density profile lead to a more gradual neutralization process and, in turn, results in a smaller emittance growth.[14]

There are other limitations of this scheme in addition to a deterioration due to transient effects during the beam entry into and exit from the plasma plug. As the beam transversely focuses after passing thorough the plasma plug, the transverse electron (and ion beam) temperature increases due to the compression and can reach very high values.[16] As a result, the electron Debye length can become comparable with the beam radius, and the degree of charge neutralization is reduced considerably. This may result in poor beam focusing. Including gas ionization by the beam ions does not significantly improve the neutralization, mainly because the electrons, which are produced by ionization, are concentrated in the beam path, whereas for effective neutralization of the ion beam pulse, the supply of electrons should be from outside the beam.[14]

Therefore, neutralized ballistic focusing typically requires the presence of background plasma in and around the beam pulse path for good charge neutralization. Reference 16 showed that hot electrons cannot neutralize the beam well enough; therefore, any electron heating due to beam-plasma interactions has to be minimized. The presence of cold, "fresh" plasma in the beam path provides the minimum space-charge potential and the best option for neutralized ballistic focusing. Experimental studies of ballistic transverse focusing have confirmed that the best results are achieved when both a plasma plug and a bulk plasma are used for

charge neutralization.[8,11] Hence, in the following we only study the case when a large amount of cold background plasma is available everywhere on the beam path.

The application of a solenoidal magnetic field allows additional control and focusing of the beam pulse.[15] A strong magnetic lens with a magnetic field up to a few Tesla can effectively focus beams in short distances order of a few tens of centimeters. However, due to the very strong magnetic field in the solenoid, the magnetic field leaking outside the solenoid can affect the degree of charge and current neutralization. In this paper, we show that even a small solenoidal magnetic field, typically less than 100 G, strongly changes the self-magnetic and self-electric fields in the beam pulse propagating in a background plasma. Such values of magnetic field can be present over distances of a few meters from the strong solenoid, and thereby affect the focusing of the beam pulse. Moreover, a small solenoidal magnetic field can be applied to optimize propagation of a beam pulse through a background plasma over long distances.

In Refs. 18 and 19, the response of a magnetized plasma to intense ion beam injection was studied while neglecting electron inertia effects, which corresponded to magnetic fields of a few Tesla in ion ring devices. In the present paper, we analyze the opposite limit, corresponding to small values of magnetic field. In the collisionless limit and without an applied solenoidal magnetic field, the return current is driven by an inductive electric field which is balanced by electron inertia effects.[20] Taking electron inertia effects into account allows us to study the transition from the limit where the solenoidal magnetic field is small, i.e., where the presence of the applied solenoidal magnetic field begins to affect the return current in the plasma, and to determine the range of magnetic field values which strongly affect the self-electric and self-magnetic fields of a beam pulse propagating in a background plasma. This allows us to study the beam pulse evolution over a wide range of solenoidal magnetic field strengths, from approximately zero to very large values, such as when the beam pulse encounters an applied solenoidal magnetic lens. Beam pulse propagation in a background plasma immersed in an applied solenoidal magnetic field has been studied both analytically and numerically using two different particle-in-cell codes to crosscheck the validity of the results.

This paper is a considerably extended version of our earlier letter[21] on this topic. In the present paper an analytic model is developed to describe the self-electromagnetic fields of a finite-length beam pulse propagating in a cold background plasma in a solenoidal magnetic field. Previously, we developed an analytic model to describe the current neutralization of a beam pulse propagating in a background plasma[20,22] without an applied magnetic field. These studies provided important scaling laws for the degrees of charge and current neutralization,[23,24] as well as served as a computationally efficient tool for describing relativistic electron beam transport in collisionless plasma for modeling of the electromagnetic Weibel instability.[22]

The electron response time to an external charge perturbation is determined by the electron plasma frequency, $\omega_{pe}=(4\pi e^2 n_p/m)^{1/2}$, where n_p is the background plasma density. Therefore, as the beam pulse enters the background plasma, the plasma electrons tend to neutralize the beam pulse on a time scale of order ω_{pe}^{-1}. Typically, the beam pulse propagation duration through the background plasma is long compared with ω_{pe}^{-1}. For electron beam pulses, some instabilities can develop very fast on a time scale comparable to the plasma period, $2\pi/\omega_{pe}$. However, if the beam density is small compared to the plasma density the instabilities' growth rates are also small compared to the plasma frequency.[22] As a result, after the beam pulse passes through a short transition region, the plasma disturbances are stationary in the beam frame. In a previous study, we have developed reduced nonlinear models, which describe the stationary plasma disturbance (in the beam frame) excited by the intense ion beam pulse.[13,20] In these calculations,[20] we investigated the nonlinear quasiequilibrium properties of an intense, long ion beam pulse propagating through a cold, background plasma, assuming that the beam pulse duration is much longer than $2\pi/\omega_{pe}$, i.e., $\tau_b\omega_{pe}\gg 2\pi$, where τ_b is the beam pulse duration. In a subsequent study,[13] we extended the previous results to general values of the parameter $\tau_b\omega_{pe}$. Theoretical predictions agree well with the results of calculations utilizing several particle-in-cell (PIC) codes.[13,20]

The model predicts very good charge neutralization during quasisteady-state propagation, provided the beam is nonrelativistic and the beam pulse duration and the beam current rise time is much longer than the electron plasma period, i.e., $\tau_b\omega_{pe}\gg 2\pi$. Thus, the degree of charge neutralization depends on the beam pulse duration and plasma density, and is independent of the beam current (if $n_p > n_b$). However, the degree of beam current neutralization depends on both the background plasma density and the beam current. The beam current can be neutralized by the electron return current. The beam charge is neutralized mostly by the action of the electrostatic electric field. In contrast, the electron return current is driven by the inductive electric field generated by the inhomogeneous magnetic flux of the beam pulse in the reference frame of the background plasma. Electrons are accelerated in the direction of beam propagation for ion beams and in the opposite direction for electron beams. From the charge density continuity equation, $\partial\rho/\partial t+\nabla\cdot J=0$ $[\rho=e(n_p+Z_b n_b-n_e)]$, it follows that if the electrons neutralize the current they will neutralize the charge as well. The inductive electric field penetrates into the plasma over distances of order the skin depth c/ω_{pe}, where c is the speed of light. If the beam radius, r_b, is small compared with the skin depth c/ω_{pe}, the electron return current is distributed over distances of order c/ω_{pe}. As a result, the electron return current is about $r_b\omega_{pe}/c$ times smaller than the beam current. Consequently, the beam current is neutralized by the electron current, provided the beam radius is large compared with the electron skin depth, i.e., $r_b > c/\omega_{pe}$, and is not neutralized in the opposite limit. This condition can be written as $I_b > 4.25\beta_b n_b/n_p$ kA, where β_b is the beam velocity normalized to the speed of light, and n_b is the beam density.

This model has been extended to include the additional effects of gas ionization during beam propagation in a background gas. Accounting for plasma production by gas ionization yields a larger self-magnetic field of the ion beam com-

pared to the case without ionization, and a wake of the current density and self-magnetic field are generated behind the beam pulse.[25] In Ref. 25, beam propagation in a dipole magnetic field configuration and background plasma has also been studied.

In the presence of an applied solenoidal magnetic field, however, the system of equations describing the self-magnetic field becomes much more complicated. A high solenoidal magnetic field inhibits radial electron transport, and the electrons move primarily along the magnetic field lines. For high-intensity beam pulses propagating through a background plasma with pulse duration much longer than the electron plasma period, one is tempted to assume that the quasineutrality condition holds, $n_e \cong n_p + Z_b n_b$, where n_e is the electron density, n_b is the density of the beam pulse, $Z_b e$ is ion charge for the beam ions, whereas $Z_b = -1$ for electron beams, and n_p is the density of the background ions (assumed unperturbed by the beam). In the limit of a strong magnetic field, the plasma electrons are attached to the magnetic field lines and their motion is primarily along the magnetic field lines. For one-dimensional electron motion, the charge density continuity equation, $\partial\rho/\partial t + \nabla\cdot\mathbf{J} = 0$, combined with the quasineutrality condition $[\rho = e(n_p + Z_b n_b - n_e) \cong 0]$ and absence of external current yields $\mathbf{J} \cong \mathbf{0}$. Therefore, in the limit of a strong solenoidal magnetic field, the beam current can be expected to be completely neutralized.

However, the above description fails to account for the electron rotation that develops in the presence of a solenoidal magnetic field. Due to the small inward radial electron motion, the electrons can enter into the region of smaller solenoidal magnetic flux. Due to the conservation of canonical angular momentum, the electrons start *spinning with a very high azimuthal velocity*, which is much larger than the ion beam rotation velocity. This spinning produces many unexpected effects.

The first effect is the dynamo effect.[26] If the magnetic field is attached to the electron flow, the electron rotation bends the solenoidal magnetic field lines and generates an azimuthal self-magnetic field in the beam pulse. (Note, though, that when electron inertia effects are taken into account the generalized electron vorticity is frozen into the plasma electron flow, rather than simply the magnetic field lines being frozen into the electron flow, as discussed in the next section.) Moreover, the electron rotation generates a self-magnetic field that is much larger than in the limit with no applied field. The second effect is the generation of a large radial electric field. Because the $v_\phi \times B_z$ force should be balanced by a radial electric field, the spinning results in a plasma polarization, and produces a much larger self-electric field than in the limit with no applied field. The total force acting on the beam particles now can change from always *focusing*[20] in the limit with no applied solenoidal magnetic field, to *defocusing* at higher values of the solenoidal magnetic field. In particular, an optimum value of magnetic field for long-distance transport of a beam pulse, needed, for example, in inertial fusion applications,[17] can be chosen where the forces nearly cancel. The third unexpected effect is that the joint system consisting of the ion beam pulse and the background plasma acts as a paramagnetic medium, i.e., the solenoidal magnetic field is enhanced inside of the ion beam pulse.

With a further increase in the magnetic field value, the beam pulse can excite strong electromagnetic perturbations, including whistler waves, corresponding to longer wavelengths,[18,27] and lower-hybrid-like or helicon waves,[28,29] corresponding to shorter wavelengths. Both wave perturbations propagate nearly perpendicular to the beam propagation direction. A similar excitation of helicon waves during fast penetration of the magnetic field due to the Hall effect in high energy plasma devices, such as, plasma opening switches and Z pinches, has been observed in Refs. 30. Here, we consider relatively short ion pulses with pulse duration $\tau_b < 2\pi/\omega_{pi}$, where ω_{pi} is the background ion plasma frequency, so that the background plasma ion response can be neglected. For longer ion pulses, the plasma ion response may effect the plasma return current.[11,31,32]

The organization of this paper is as follows: In Sec. II, the basic equations and model are discussed. Section III provides a comparison between analytic theory and particle-in-cell simulations results. In Sec. IV, the dependence of the radial force acting on the beam particles on the strength of the solenoidal magnetic field is discussed. Finally, Sec. V describes the excitation of electromagnetic perturbations by the beam pulse, including whistler waves and lower-hybrid-like (helicon) waves. In a follow-up publication the limit of strong magnetic field will be discussed.[33]

II. BASIC EQUATIONS

The electron fluid equations together with Maxwell's equations comprise a complete system of equations describing the electron response to the propagating ion beam pulse. The electron fluid equations consist of the continuity equation,

$$\frac{\partial n_e}{\partial t} + \nabla\cdot(n_e \mathbf{V}_e) = 0, \tag{1}$$

and the force balance equation,

$$\frac{\partial \mathbf{V}_e}{\partial t} + (\mathbf{V}_e\cdot\nabla)\mathbf{V}_e = -\frac{e}{m}\left(\mathbf{E} + \frac{1}{c}\mathbf{V}_e \times \mathbf{B}\right), \tag{2}$$

where $-e$ is the electron charge, m is the electron rest mass, and $\mathbf{V}_e$ is the electron flow velocity. Maxwell's equations for the self-generated electric and magnetic fields, $\mathbf{E}$ and $\mathbf{B}$, are given by

$$\nabla \times \mathbf{B} = \frac{4\pi e}{c}(Z_b n_b \mathbf{V}_b - n_e \mathbf{V}_e) + \frac{1}{c}\frac{\partial \mathbf{E}}{\partial t}, \tag{3}$$

$$\nabla \times \mathbf{E} = -\frac{1}{c}\frac{\partial \mathbf{B}}{\partial t}, \tag{4}$$

where $\mathbf{V}_b$ is the ion beam velocity, n_e and n_b are the number densities of the plasma electrons and beam ions, respectively, and Z_b is the ion charge state for the beam ions, whereas $Z_b = -1$ for electron beams.

We assume that the beam pulse moves with constant velocity V_b along the z-axis. We look for stationary solutions

in the reference frame of the moving beam, i.e., where all quantities depend on t and z exclusively through the combination $(V_b t - z)$. We further consider cylindrically symmetric, long beam pulses with length, l_b, and radius, r_b, satisfying

$$l_b \gg V_b/\omega_{pe}, \quad l_b \gg r_b, \tag{5}$$

where $\omega_{pe}=(4\pi e^2 n_e/m)^{1/2}$ is the electron plasma frequency. We also assume that the fields and electron flow velocity and density are in steady state in a reference frame moving with the beam pulse. We introduce the vector potential,

$$\mathbf{B} = \nabla \times \mathbf{A}, \tag{6}$$

and make use of the transverse Coulomb gauge, $\nabla_\perp \cdot \mathbf{A} = \mathbf{0}$. For axisymmetric geometry, this gives $A_r=0$. The azimuthal magnetic field is

$$B_\phi = -\frac{\partial A_z}{\partial r}, \tag{7}$$

and the perturbed (by the plasma) magnetic field components are

$$B_z = \frac{1}{r}\frac{\partial (rA_\phi)}{\partial r}, \quad B_r = -\frac{\partial A_\phi}{\partial z}. \tag{8}$$

For long beams with $l_b \gg V_b/\omega_{pe}$, the displacement current [the final term on the right-hand side of Eq. (3)] is of order $(V_b/\omega_{pe} l_b)^2 \ll 1$ compared to the electron current. Because $l_b \gg r_b$ is assumed, the terms on the left-hand side of Eqs. (3) of order $(r_b/l_b)^2$ are neglected, as well. This gives

$$-\frac{1}{r}\frac{\partial}{\partial r}\left(r\frac{\partial A_z}{\partial r}\right) = \frac{4\pi e}{c}(Z_b n_b V_{bz} - n_e V_{ez}) \tag{9}$$

and

$$-\frac{\partial}{\partial r}\left[\frac{1}{r}\frac{\partial (rA_\phi)}{\partial r}\right] = \frac{4\pi e}{c}(Z_b n_b V_{b\phi} - n_e V_{e\phi}). \tag{10}$$

The electron momentum equation, Eq. (2), can be solved to obtain the three components of electron velocity $V_{ez}, V_{er}, V_{e\phi}$. However, it is easier to use conservation of the generalized vorticity,[20,22,30,34] which states that the circulation C of the canonical momentum,

$$C \equiv \oint (\mathbf{p}_e - e\mathbf{A}/c) \cdot \delta\mathbf{r} \tag{11}$$

taken along a closed loop, which is "frozen-in" and moving together with the electron fluid, remains constant. Applying Thompson's theorem, the circulation defined in Eq. (11) can be rewritten as the surface integral of the generalized vorticity

$$\begin{aligned} C &= \oint (\mathbf{p}_e - e\mathbf{A}/c) \cdot \delta\mathbf{r} \\ &= \int \nabla \times (\mathbf{p}_e - e\mathbf{A}/c) \cdot \delta\mathbf{S} \\ &\equiv \int \mathbf{\Omega} \cdot \delta\mathbf{S}, \end{aligned} \tag{12}$$

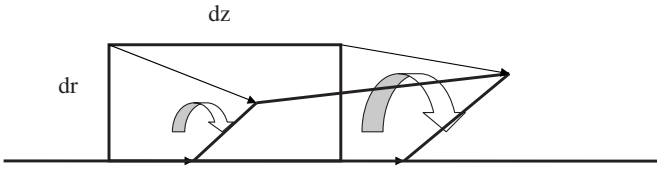

FIG. 1. Schematic of the differential rotation of fluid elements near the symmetry axis.

where $\delta\mathbf{S}$ is the fluid surface element, and the generalized vorticity is defined as

$$\mathbf{\Omega} = \nabla \times (\mathbf{p}_e - e\mathbf{A}/c). \tag{13}$$

If electron inertia terms are neglected, the electron mechanical momentum can also be neglected in the expression for the generalized vorticity, which gives $\mathbf{\Omega} \approx -e\mathbf{B}/c$. The conservation of generalized vorticity then becomes the well-known expression for the conservation of magnetic flux through a fluid contour ($C=\oint \mathbf{B}\cdot\delta\mathbf{S}=$const.), e.g., see Ref. 35.

Equation (12) can be rewritten in the differential form[20]

$$\frac{\partial \mathbf{\Omega}}{\partial t} + (\mathbf{V_e}\cdot\nabla)\mathbf{\Omega} = -\mathbf{\Omega}(\nabla\cdot\mathbf{V_e}) + (\mathbf{\Omega}\cdot\nabla)\mathbf{V_e}. \tag{14}$$

Substituting $\nabla\cdot\mathbf{V_e}$ into Eq. (14) from the continuity equation (1),

$$\nabla\cdot\mathbf{V_e} = -\frac{1}{n_e}\frac{\partial n_e}{\partial t} - \frac{\mathbf{V_e}}{n_e}\cdot\nabla n_e, \tag{15}$$

gives

$$\left(\frac{\partial}{\partial t} + \mathbf{V_e}\cdot\nabla\right)\left(\frac{\mathbf{\Omega}}{n_e}\right) = \left(\frac{\mathbf{\Omega}}{n_e}\cdot\nabla\right)\mathbf{V_e}. \tag{16}$$

This is a generalization of the "frozen-in" condition for the magnetic field lines, when electron inertia terms are neglected.[35]

As an example of application of the generalized vorticity law, we derive the magnetic dynamo effect using both integral and differential forms of the conservation of generalized vorticity, given by Eq. (12) and Eq. (16), respectively. Consider a small element of the electron fluid of size $drdz$, positioned in a plane of constant ϕ; then $\int\mathbf{\Omega}\cdot\delta\mathbf{S}=(\Omega_\phi drdz)_0$, as shown in Fig. 1. In the next time interval, $t+dt$, the fluid element moves and rotates. Due to the differential rotation $\partial V_{e\phi}/\partial z$, the sides of the element rotate differently, and the surface element opens in the z-direction. In the next time interval, $\int\mathbf{\Omega}\cdot\delta\mathbf{S}=-\Omega_z drdz\partial V_{e\phi}/\partial z dt+(\Omega_\phi drdz)_1$. Using the fact that the electron density is conserved in the fluid element, $drdzn_e$, the time derivative of the azimuthal component of vorticity, $(\Omega_{\phi 1}-\Omega_{\phi 0})/dt$, can be written as

$$\frac{d}{dt}\frac{\Omega_\phi}{n_e} = \frac{1}{n_e}\Omega_z\frac{\partial V_{e\phi}}{\partial z}. \tag{17}$$

This result can also be derived directly by taking the azimuthal projection of Eq. (16) and neglecting the small radial contribution on the right-hand side, because $\Omega_r \ll \Omega_z$.

For simplicity, in the following we consider the most practically important case when the plasma density is large

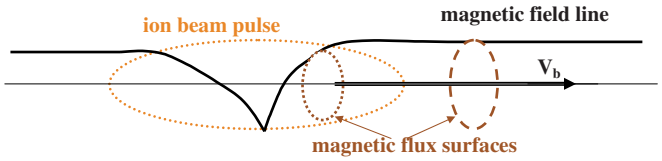

FIG. 2. (Color online) Schematic of magnetic field generation due to the dynamo effect. The magnetic field line is shown by the black solid line; a contour attached to the electron fluid element is shown by the brown dashed line in front of the beam pulse; and the dotted brown line indicates this contour inside of the ion beam pulse, the outline of which is shown by the orange, thin dotted line. The radial electron displacement generates a poloidal rotation; the poloidal rotation twists the solenoidal magnetic field and generates the poloidal magnetic field.

$n_p \gg n_b$ so that the changes in n_e can be neglected in Eq. (16). Also because $n_p \gg n_b$, the effects of electron flows are small compared to the beam motion ($V_{ez} \ll V_b$), and we approximate $d/dt \approx V_b \partial/\partial z$. Substituting into Eq. (17), and integrating with zero initial conditions in front of the beam pulse gives

$$\Omega_\phi = \frac{\Omega_z V_{e\phi}}{V_b}. \tag{18}$$

Here, we made use of the fact that $\Omega_z = -eB_z/c$ is approximately constant. From Eq. (13), it follows that $\Omega_\phi \simeq -\partial(mV_{ez} - eA_z/c)/\partial r$, where only the radial derivatives are taken into account, due to the approximation of long beam pulses in Eq. (5). Substituting the expressions for Ω_ϕ and Ω_z into Eq. (18), and integrating radially gives

$$V_{ez} = \frac{e}{mc}A_z + \frac{eB_z}{mcV_b}\int_r^\infty V_{e\phi} dr. \tag{19}$$

The first term on the right-hand side of Eq. (19) describes the conservation of canonical momentum in the absence of magnetic field; the second term describes the magnetic dynamo effect, i.e., the generation of azimuthal magnetic field due to the rotation of magnetic field lines,[26] as shown in Fig. 2. Note that, if the inertia effects are neglected, Eq. (18) describes the magnetic field "frozen in" the electron flow, $B_\phi = B_z V_{e\phi}/V_b$.

Substituting $V_{e\phi}$ from Ampere's law in Eq. (10), and assuming that the velocity of the beam rotation is small compared to the rotation velocity of the plasma electrons, gives

$$\int_r^\infty V_{e\phi} dr = -\frac{c}{4\pi e n_p}\frac{1}{r}\frac{\partial(rA_\phi)}{\partial r} + \int_r^\infty Z_b \frac{n_b}{n_p} V_{b\phi} dr. \tag{20}$$

Substituting Eq. (20) into Eq. (19) then gives

$$V_{ez} = \frac{e}{mc}A_z - \frac{B_z}{4\pi m V_b n_e}\frac{1}{r}\frac{\partial(rA_\phi)}{\partial r} + \frac{eB_z}{mcV_b}\int_r^\infty Z_b \frac{n_b}{n_p} V_{b\phi} dr. \tag{21}$$

Similarly, from the z projection of Eq. (16), we obtain

$$\frac{\partial}{r\partial r} r(mV_{e\phi} - eA_\phi/c) = -\frac{eB_z}{cV_b}\left(V_b \frac{n_e - n_p}{n_p} - V_{ez}\right), \tag{22}$$

and accounting for quasineutrality, $n_e - n_p = Z_b n_b$, and substituting the expression for the current $J_z = Z_b e n_b V_b - e n_p V_{ez}$ gives

$$mV_{e\phi} - eA_\phi/c = \frac{B_z}{cV_b n_p r}\int_r^\infty J_z r dr. \tag{23}$$

Equation (23) describes the conservation of canonical angular momentum

$$mV_{e\phi} = \frac{e}{c}(A_\phi + \delta r B_z), \tag{24}$$

where δr is the change in the radial position of the electron fluid element inside of the beam pulse compared to the initial radial position in front of the beam pulse. Indeed, because of the conservation of current, $\nabla \cdot \mathbf{J} = 0$, it follows that $\int_r^\infty J_z r dr = er\int_z^\infty n_e V_{er} dz = eV_b r n_p \delta r$, where δr is the change in the radial position of a contour immersed in the electron fluid. Equation (23) also describes the conservation of vorticity flux in the z-direction through a circle in the azimuthal direction, $\int \boldsymbol{\Omega} \cdot \delta \mathbf{S} = 2\pi \int_0^r r dr \Omega_z = 2\pi \int_0^r r dr d[r(mV_{e\phi} - eA_\phi/c)]/r dr = 2\pi r(mV_{e\phi} - eA_\phi/c) - \pi r^2 eB_z/c = \text{const}$.

Making use of Ampere's equation in the z-direction gives $\int_r^\infty J_z r dr = (cr/4\pi)\partial A_z/\partial r$, and

$$mV_{e\phi} - \frac{e}{c}A_\phi = \frac{B_z}{4\pi V_b n_p}\frac{\partial A_z}{\partial r}. \tag{25}$$

Substituting Eqs. (19) and (25) into the corresponding components of Ampere's equation then gives

$$-\frac{1}{r}\frac{\partial}{\partial r}\left(r\frac{\partial A_z}{\partial r}\right) = \frac{4\pi e}{c}\left[Z_b n_b V_{bz} - \frac{e}{mc}n_e A_z + \frac{B_z}{4\pi m V_b}\frac{1}{r}\frac{\partial(rA_\phi)}{\partial r} + \frac{eB_z}{mcV_b}\int_r^\infty Z_b \frac{n_b}{n_p} V_{b\phi} dr\right], \tag{26}$$

and

$$-\frac{\partial}{\partial r}\left[\frac{1}{r}\frac{\partial(rA_\phi)}{\partial r}\right] = \frac{4\pi e}{c}\left(Z_b n_b V_{b\phi} - \frac{e}{mc}n_e A_\phi - \frac{B_z}{4\pi m V_b}\frac{\partial A_z}{\partial r}\right). \tag{27}$$

As we shall see in the next section, under conditions of interest, the electron rotation is of order the electron cyclotron frequency times the ratio of the beam density to the plasma density, which is much larger than the ion rotation, which is given by the ion cyclotron frequency and the last term on the right-hand side of Eq. (26) can be neglected. In general, analysis shows that the electron inertia terms are important if

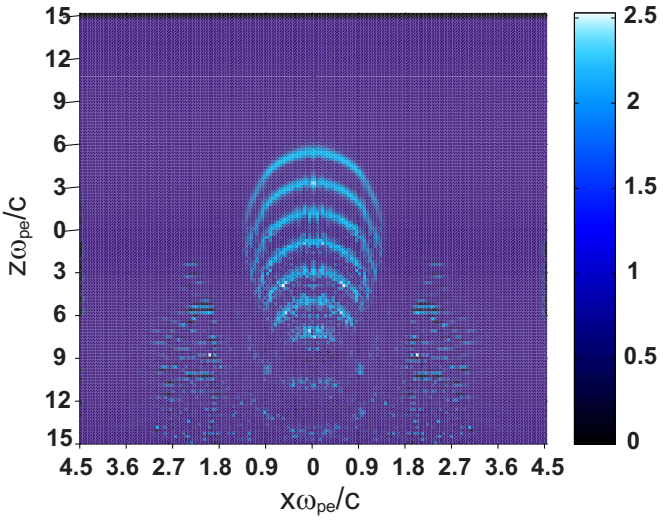

FIG. 3. (Color online) The electron density perturbation caused by an ion beam pulse moving with velocity $V_b=0.5c$ along the z-axis. The beam density is one-half of the background plasma density; the beam profile is flattop with smooth edges; the beam radius is $r_b=1.5c/\omega_{pe}$; and the beam half length is $l_b=7.5c/\omega_{pe}$.

$$\frac{\omega_{ec} r_b}{V_b} < \sqrt{\frac{M}{m}},$$

in the opposite limit of the electron motion can be described in pure drift approximation.

III. COMPARISON OF ANALYTIC THEORY AND PARTICLE-IN-CELL SIMULATIONS

Figures 3 and 4 show the simulation results obtained from the particle-in-cell (PIC) code EdPIC (Ref. 20) for the density and magnetic field of an ion beam pulse propagating with beam velocity $V_b=0.5c$ in slab geometry, whereas Figs. 5 and 6 show the simulation results obtained from the LSP code, with $V_b=0.33c$.[36] In all simulations beams enter the plasma in the presence of a uniform solenoidal magnetic field. After some transitional period, plasma perturbations reach a quasisteady-state in the beam frame. We have performed the PIC simulations in slab geometry, because the numerical noise tends to be larger in cylindrical geometry

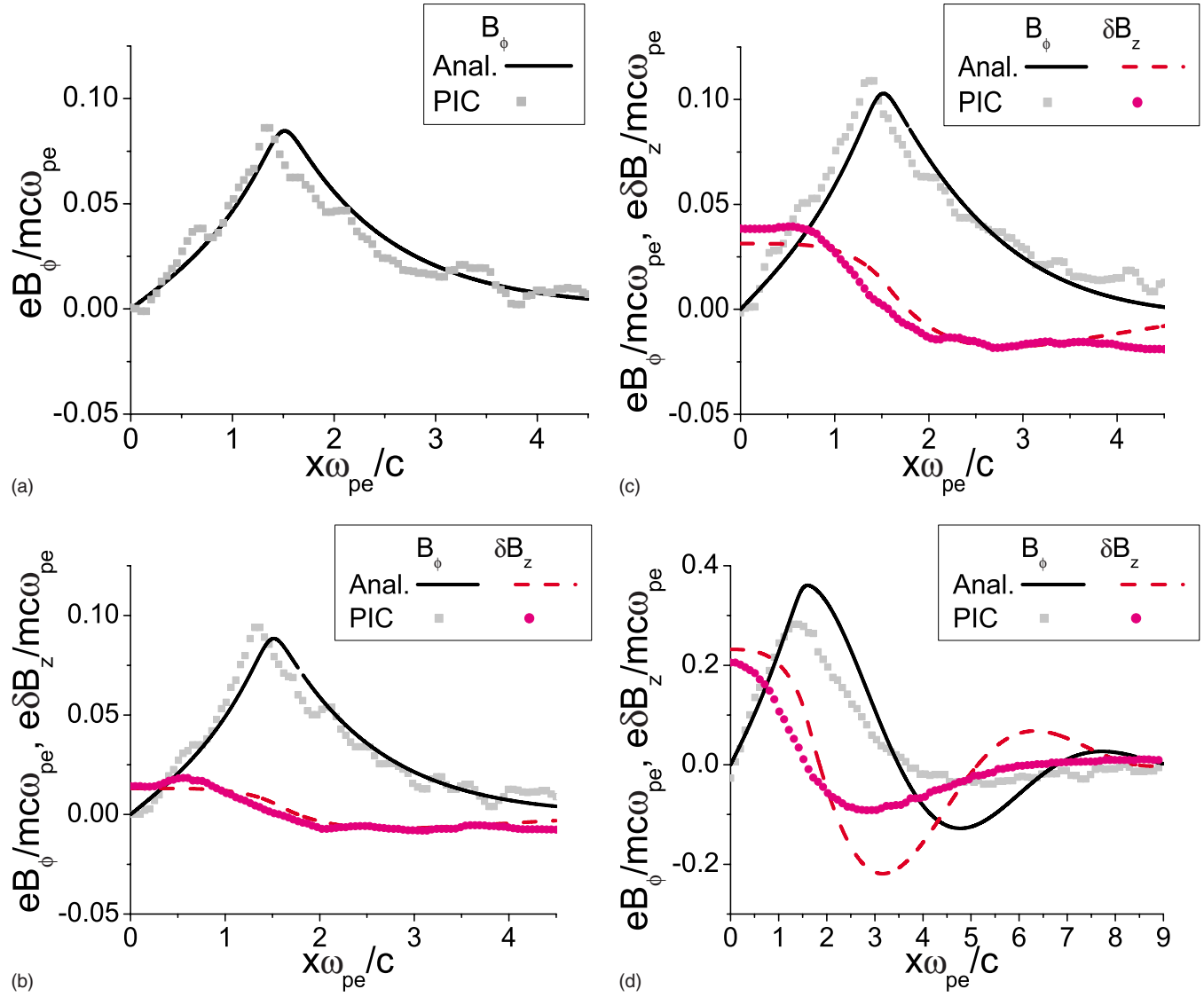

FIG. 4. (Color online) Comparison of analytic theory and EdPIC particle-in-cell simulation results for the self-magnetic field and the perturbations in the solenoidal magnetic field in the center slice of the beam pulse. The beam parameters are the same as in Fig. 3. The beam velocity $V_b=0.5c$. The values of applied solenoidal magnetic field correspond to the ratio of cyclotron to plasma frequency ω_{ce}/ω_{pe}: (a) 0; (b) 0.25; (c) 0.5; and (d) 1.

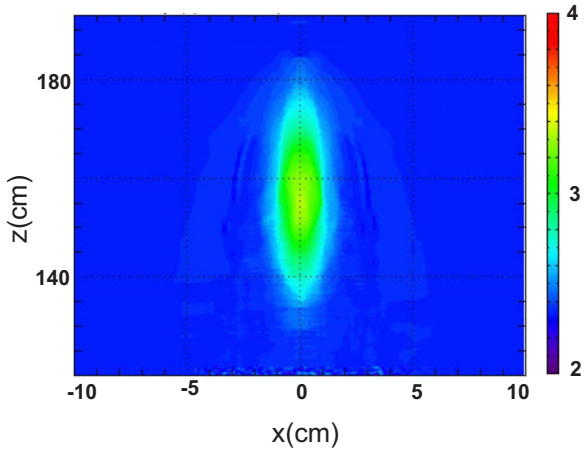

FIG. 5. (Color online) The electron density perturbation caused by an ion beam pulse moving with velocity $V_b=0.33c$ along the z-axis. The beam density profile is Gaussian with $r_b=1$ cm, $l_b=17$ cm, and $n_{b0}=n_p/2=1.2\times10^{11}$ cm^{-3}.

due to the singularity on the axis ($r=0$). In Fig. 3, the beam density is one-half of the background plasma density; the beam profile has a flat top with smooth edges; the beam radius corresponds to $r_b=1.5c/\omega_{pe}$; and the beam half length is $l_b=7.5c/\omega_{pe}$, lead ions were assumed, however, and ion motion was not important for short beam pulses. Figure 3 shows that large-amplitude plasma waves are excited by the beam head. The plasma waves are electrostatic, and, therefore, the plasma waves do not have an effect on the structure of the self-magnetic field of the beam pulse,[20] except that the local value of the electron density is different from the predictions of the quasineutrality condition ($n_e=Z_bn_b+n_p$) and affects the value of the return current en_eV_{ez}. Such large density perturbations are not accounted for in linear analytic theory ($n_b \ll n_p$), which is the reason for the difference between the PIC simulations and the analytic predictions, as will be shown below. Note that the presence of the solenoidal magnetic field results in an increase of the self-magnetic field. This is due to the magnetic dynamo effect caused by the electron rotation, as discussed above (see also Fig. 2).

Another unusual effect is that the system consisting of the beam pulse together with the background plasma acts paramagnetically; the solenoidal magnetic field is larger in the center of the beam pulse than the initial value of the applied magnetic field. This effect can be found to originate from Eqs. (26) and (27) in the limit where the skin depth is large compared with the beam radius ($c/\omega_{pe} \gtrsim r_b$). In this limit, the terms proportional to the return current n_eA_ϕ on the right-hand side of Eq. (27) can be neglected compared with the terms on the left-hand side. Without taking into account contributions from the ions, and neglecting the term n_eA_ϕ, Eq. (27) can then be integrated from r to ∞, assuming that $A_\phi=0$ as $r\to\infty$. This gives for the perturbation in the solenoidal magnetic field

$$\delta B_z=\frac{1}{r}\frac{\partial(rA_\phi)}{\partial r}=\frac{4\pi e}{c}\left(\frac{B_zA_z}{4\pi mV_b}\right). \tag{28}$$

Note that δB_z is positive, i.e., the combination of the beam and plasma acts paramagnetically! In the follow-up research,[37] we found that the beam plus plasma system response strongly depends on parameter $\omega_{ce}/\beta_b\omega_{pe}$. *If* $\omega_{ce}/\beta_b\omega_{pe}<1$, *the response is paramagnetic, if* $\omega_{ce}/\beta_b\omega_{pe}>1$, *the response is diamagnetic.*

Substituting Eq. (28) into Eq. (26) gives

$$-\frac{1}{r}\frac{\partial}{\partial r}\left(r\frac{\partial A_z}{\partial r}\right)=\frac{4\pi e}{c}\left(Z_bn_bV_{bz}-\frac{e}{mc}n_eA_z+\frac{B_z^2}{4\pi m^2V_b^2}\frac{e}{c}A_z\right). \tag{29}$$

Note that the final positive term on the right-hand side of Eq. (29) proportional to B_z^2 describes the dynamo effect, and leads to an increase in the self-magnetic field. This increase becomes significant if

$$n_e\sim\frac{B_z^2}{4\pi mV_b^2} \tag{30}$$

or

$$\omega_{ce}\sim\omega_{pe}\frac{V_b}{c}, \tag{31}$$

where $\omega_{ce}=eB_z/mc$ is the electron cyclotron frequency. This is evident in Fig. 4 by comparing the value of the self-magnetic field in Figs. 4(a)–4(c) with Fig. 4(d).

Figure 6 shows a comparison of analytic theory and LSP (Ref. 36) particle-in-cell simulation results for the self-magnetic field, the perturbation in the solenoidal magnetic field, and the radial electric field in the ion beam pulse. The beam velocity is $V_b=0.33c$, and the beam density profile is Gaussian, $n_{b0}\exp(-r^2/r_b^2-z^2/l_b^2)$, where $r_b=1$ cm, $l_b=17$ cm, $n_{b0}=n_p/2=1.2\times10^{11}$ cm^{-3}. The background plasma density is $n_p=2.4\times10^{11}$ cm^{-3}, except for case (d), where the beam density is $n_{b0}=0.6\times10^{11}$ cm^{-3} and the plasma density is $n_p=4.8\times10^{11}$ cm^{-3}; and case (f), where $n_{b0}=0.3\times10^{11}$ cm^{-3} and the background density is $n_p=2.4\times10^{11}$ cm^{-3}. Figure 5 shows the electron density perturbation generated by the beam pulse. Because the beam head is long compared with the length V_b/ω_{pe}, the beam head does not excite any plasma waves,[20] and the quasineutrality condition $n_e=n_b+n_p$ is satisfied (compare Fig. 3 and Fig. 5).

For this choice of beam parameters, the skin depth is approximately equal to the beam radius $c/\omega_{pe}\simeq r_b$, so that the return current does not screen the beam self-magnetic field significantly. Without the applied solenoidal magnetic field, the maximum value of the magnetic field is 56 G [see Fig. 6(a)]. The analytic theory agrees well with the PIC simulation results, because in this case the theory applies even for the nonlinear case $n_b\sim n_p$.[20] The radial electric field is small and cannot be distinguished from numerical noise in the PIC simulations. For the value of the applied solenoidal magnetic field $B_{z0}=300$ G, in Fig. 6(b), the parameter $\omega_{ce}/\beta_b\omega_{pe}=0.57$, where $\beta_b=V_b/c$ is small. Therefore, the dynamo effect is insignificant according to Eq. (29). Figures 6(c) and 6(e) correspond to two and three times larger magnetic fields ($B_{z0}=600$ G and $B_{z0}=900$ G), respectively. The value of the parameter $\omega_{ce}/\beta_b\omega_{pe}=1.1, 1.7$, rises above unity, and the dynamo effect results in a considerable increase in

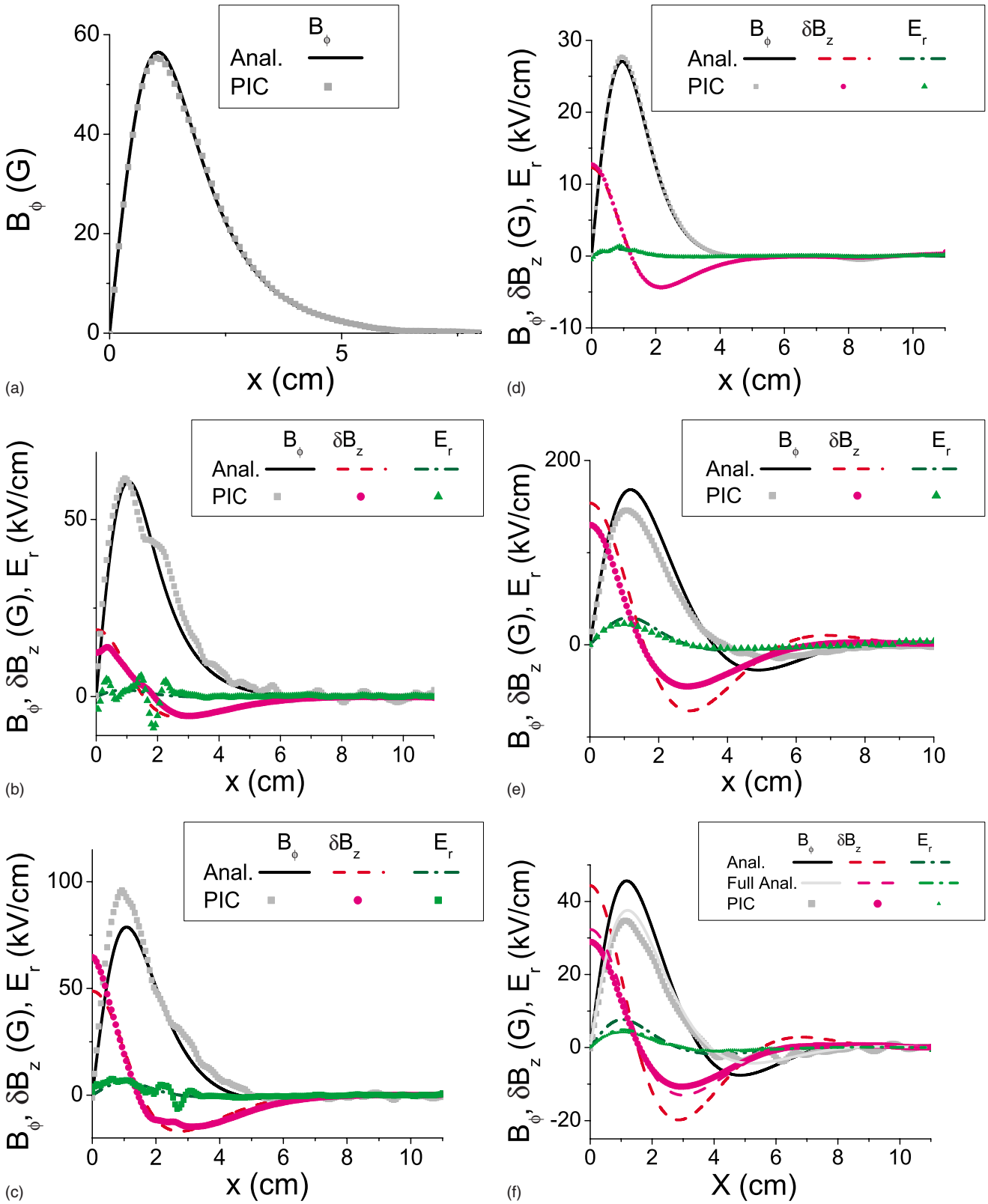

FIG. 6. (Color online) Comparison of analytic theory and LSP particle-in-cell simulation results for the self-magnetic field, perturbation in the solenoidal magnetic field, and the radial electric field in a perpendicular slice of the beam pulse. The beam parameters are the same as in Fig. 5 with $n_{b0}=n_p/2=1.2\times10^{11}$ cm^{-3}, except for (d), where $n_{b0}=n_p/8=0.6\times10^{11}$ cm^{-3}, and (f), where $n_{b0}=n_p/8=0.3\times10^{11}$ cm^{-3}. The values of the applied solenoidal magnetic field, B_{z0}, are: (a) $B_{z0}=0$ G; (b) $B_{z0}=300$ G; (c) and (d) $B_{z0}=600$ G; (e) and (f) $B_{z0}=900$ G.

the self-magnetic field of the beam, also in agreement with Eq. (29). The 20% difference between the analytic and PIC simulation results is due to the fact that the theory of the dynamo effect is linear in the parameter n_b/n_p, whereas $n_b/n_p=0.5$ in Figs. 6(b), 6(c), and 6(e). Figure 6(d) shows results for $n_b/n_p=0.125$, and the linear theory results are practically indistinguishable from the PIC simulation results. Figure 6(f) shows results for $n_b/n_p=0.125$, and the linear

theory results differs from the PIC simulation results by approximately 30%. This is due to the assumption of quasineutrality, which requires $\omega_{ce}^2/\omega_{pe}^2 \lesssim 1$ as shown below. For the conditions in Fig. 6(f), $\omega_{ce}^2/\omega_{pe}^2=0.33$, which accounts for the 30% difference from the PIC simulation results.

The radial electric field can be obtained from the radial component of the momentum balance equation (2). Neglecting the small radial electron velocity V_{er} gives

$$E_r = \frac{mV_{e\phi}^2}{er} + \frac{1}{c}(-V_{e\phi}B_z + V_{ez}B_\phi), \tag{32}$$

where $V_{e\phi}$ is given by Eq. (25). From Eq. (32) it follows that the radial electric field increases strongly with increasing solenoidal magnetic field, as is evident in Fig. 6. As shown in Sec. V, the ion dynamics can reduce radial electric field and has to be taken into account for very long beam pulses $l_b > r_b(M/m)^{1/2}$.

As the electric field increases with an increase in the applied solenoidal magnetic field, the assumption of quasineutrality may fail. To find the criterion for validity of the theory we estimate the electric field value, considering only linear terms assuming $n_b \ll n_p$. In this limit, the nonlinear terms in Eq. (32) can be neglected, which gives

$$E_r = -\frac{1}{c}V_{e\phi}B_z. \tag{33}$$

Equations (26) and (27) can be represented in dimensionless form if the following normalization is applied:

$$[r] = \delta_p \equiv \frac{c}{\omega_{pe}},$$

$$[A_z] = \frac{mcV_{bz}}{e}\frac{Z_b n_{b0}}{n_p},$$

$$[A_\phi] = B_z\delta_p\frac{Z_b n_{b0}}{n_p},$$

$$[V_{e\phi}] = \frac{eB_z\delta_p}{mc}\frac{Z_b n_{b0}}{n_p},$$

where $n_{b0}=n_b(0)$ is the on-axis value of the beam density. Some straightforward algebra applied to Eqs. (26) and (27) gives for the normalized components of vector potential, $a_z = A_z/[A_z]$ and $a_\phi = A_\phi/[A_\phi]$,

$$-\frac{1}{\rho}\frac{\partial}{\partial\rho}\left(\rho\frac{\partial a_z}{\partial\rho}\right) = \frac{n_b(r/\delta_p)}{n_{b0}} - a_z + \frac{\omega_{ce}^2}{\omega_{pe}^2\beta_b^2}\frac{1}{\rho}\frac{\partial(\rho a_\phi)}{\partial\rho}, \tag{34}$$

$$\frac{\partial}{\partial\rho}\left(\frac{1}{\rho}\frac{\partial(\rho a_\phi)}{\partial\rho}\right) = a_\phi + \frac{\partial a_z}{\partial\rho}. \tag{35}$$

Here, $\rho \equiv r/\delta_p$. Note that the solutions of Eqs. (34) and (35) depend only on two parameters: the ratio of the beam radius to the skin depth (through the beam density profile), and the parameter $\omega_{ce}^2/\omega_{pe}^2\beta_b^2$, which characterizes the dynamo effect [see Eq. (31)].

The electron rotation velocity and azimuthal magnetic field are expressed through the normalized components of vector potential according to

$$V_{e\phi} = \frac{Z_b n_{b0}}{n_p}\frac{eB_z\delta_p}{mc}\left(a_\phi + \frac{\partial a_z}{\partial\rho}\right), \tag{36}$$

$$B_\phi = -\frac{Z_b n_{b0}}{n_p}\frac{mcV_{bz}}{e\delta_p}\frac{\partial a_z}{\partial\rho}. \tag{37}$$

Substituting Eqs. (36) and (37) into Eq. (33) then gives

$$E_r = -\frac{Z_b n_{b0}}{n_p}\frac{mV_{bz}^2}{e\delta_p}\frac{\omega_{ce}^2}{\omega_{pe}^2\beta_b^2}\left[\frac{\partial a_z}{\partial\rho} + a_\phi\right]. \tag{38}$$

The quasineutrality condition requires

$$\left|\frac{\partial rE_r}{r\partial r}\right| \lesssim 4\pi e|Z_b|n_{b0}. \tag{39}$$

Substituting the estimate $\partial E_r/\partial r \sim E_r/\delta_p$ for E_r into Eq. (38), and taking the normalized vector potentials to be of order unity into Eq. (39) gives the condition

$$\frac{\omega_{ce}^2}{\omega_{pe}^2} \lesssim 1. \tag{40}$$

The reason for the condition in Eq. (40) can be explained as follows. The dielectric constant transverse to the magnetic field is given by

$$\varepsilon_\perp = 1 + \frac{\omega_{pe}^2}{\omega_{ce}^2 - \omega^2}. \tag{41}$$

In the analytic derivation, we accounted only for the plasma part of the dielectric constant [the last term on the right-hand side of Eq. (41)], and neglected the displacement current. Apparently when $\omega \ll \omega_{ce}$, this is valid only if the condition in Eq. (40) is satisfied. In order to account for a departure from the quasineutrality condition, we substitute into Eq. (22) the perturbations in the electron density according to the Poisson equation

$$(Z_b n_b - n_e + n_p) = \frac{1}{4\pi er}\frac{\partial(rE_r)}{\partial r},$$

which gives

$$\frac{\partial[r(mV_{e\phi} - eA_\phi/c)]}{r\partial r} = -\frac{B_z}{cn_pV_b}\left[-\frac{V_b\partial(rE_r)}{4\pi r\partial r} + Z_b n_b eV_b - eV_{ez}n_p\right]. \tag{42}$$

Integrating Eq. (42) with respect to r gives

$$V_{e\phi} = \frac{e}{mc}A_\phi + \frac{B_z}{mcV_b n_p r}\left[\int_r^\infty J_z r dr + \frac{rV_b E_r}{4\pi}\right]. \tag{43}$$

Substituting Eq. (33) for E_r,

$$E_r = -\frac{1}{c}V_{e\phi}B_z, \tag{44}$$

and $\int_r^\infty J_z r dr = (cr/4\pi)\partial A_z/\partial r$ into Eq. (43) then gives

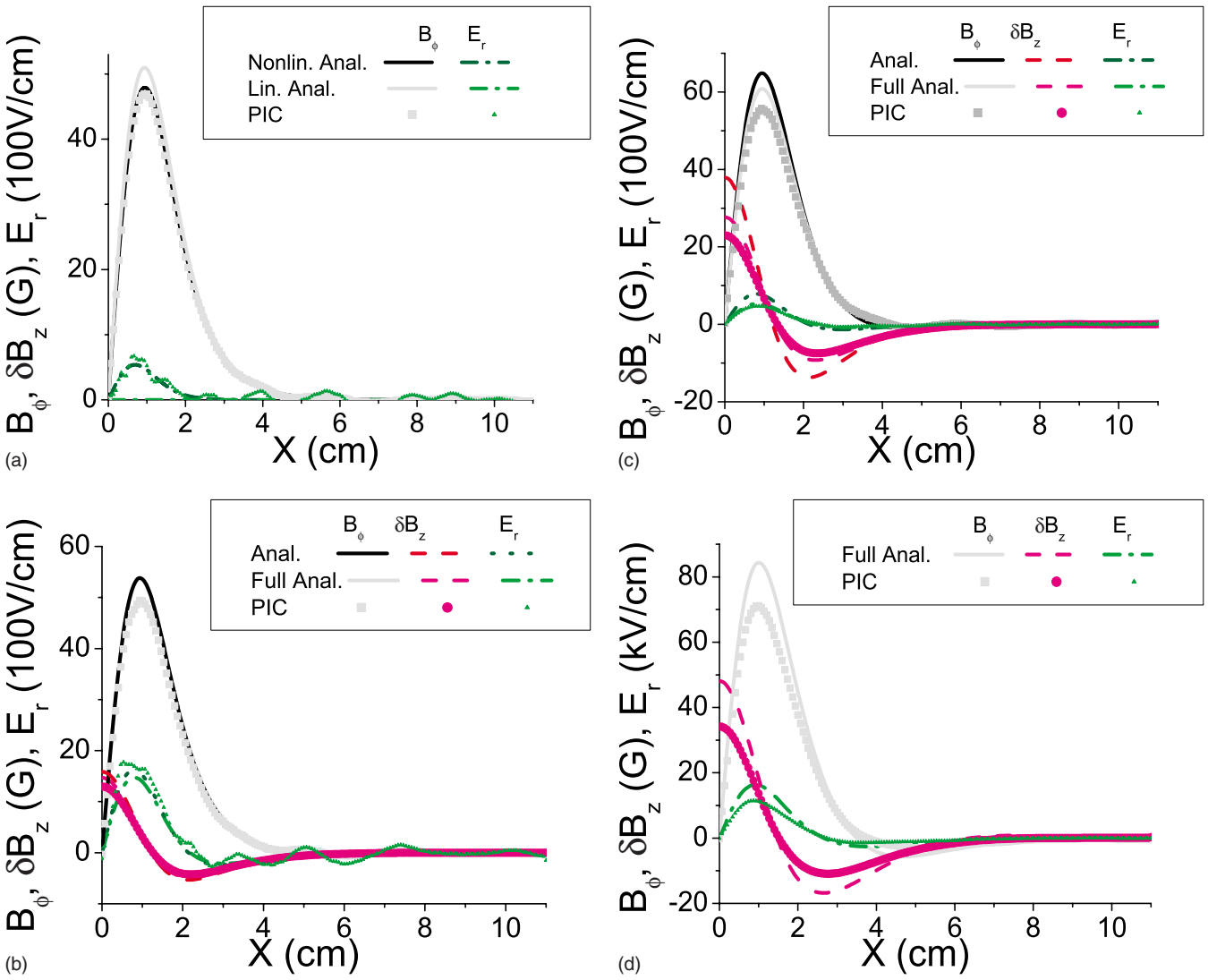

FIG. 7. (Color online) Comparison of analytic theory and LSP particle-in-cell simulation results for the self-magnetic field, perturbation in the solenoidal magnetic field, and the radial electric field in a perpendicular slice of the beam pulse. The beam velocity is $V_b=0.808c$. The plasma and beam parameters are $n_p=4.8\times10^{11}$ cm^{-3}, $n_{b0}=0.5\times10^{11}$ cm^{-3}. The values of the applied solenoidal magnetic field, B_{z0}, are: (a) $B_{z0}=0$ G; (b) $B_{z0}=900$ G; (c) $B_{z0}=1800$ G; and (d) $B_{z0}=3600$ G.

$$V_{e\phi}\left(1+\frac{\omega_{ce}^2}{\omega_{pe}^2}\right)=\frac{e}{mc}A_\phi+\frac{B_z}{4\pi mV_bn_p}\frac{\partial A_z}{\partial r}. \tag{45}$$

Equation (26) remains the same, but Eq. (27) is modified to become

$$-\left(1+\frac{\omega_{ce}^2}{\omega_{pe}^2}\right)\frac{\partial}{\partial r}\left[\frac{1}{r}\frac{\partial(rA_\phi)}{\partial r}\right]=\frac{4\pi e}{c}\left(Z_bn_bV_{b\phi}-\frac{e}{mc}n_eA_\phi-\frac{B_z}{4\pi mV_b}\frac{\partial A_z}{\partial r}\right). \tag{46}$$

The equations for the normalized vector potentials become

$$-\frac{1}{\rho}\frac{\partial}{\partial\rho}\left(\rho\frac{\partial a_z}{\partial\rho}\right)=\frac{n_b(r/\delta_p)}{n_{b0}}-a_z+\frac{\omega_{ce}^2}{\omega_{pe}^2\beta_b^2}\frac{1}{\rho}\frac{\partial(\rho a_\phi)}{\partial\rho}, \tag{47}$$

$$\left(1+\frac{\omega_{ce}^2}{\omega_{pe}^2}\right)\frac{\partial}{\partial\rho}\left[\frac{1}{\rho}\frac{\partial(\rho a_\phi)}{\partial\rho}\right]=a_\phi+\frac{\partial a_z}{\partial\rho}. \tag{48}$$

The electron rotation velocity, azimuthal magnetic field, and radial electric field are then expressed through the normalized components of vector potential according to

$$V_{e\phi}=\frac{Z_bn_{b0}}{n_p\left(1+\frac{\omega_{ce}^2}{\omega_{pe}^2}\right)}\frac{eB_z\delta_p}{cm}\left(a_\phi+\frac{\partial a_z}{\partial\rho}\right), \tag{49}$$

$$B_\phi=-\frac{Z_bn_{b0}}{n_p}\frac{mcV_{bz}}{e\delta_p}\frac{\partial a_z}{\partial\rho}, \tag{50}$$

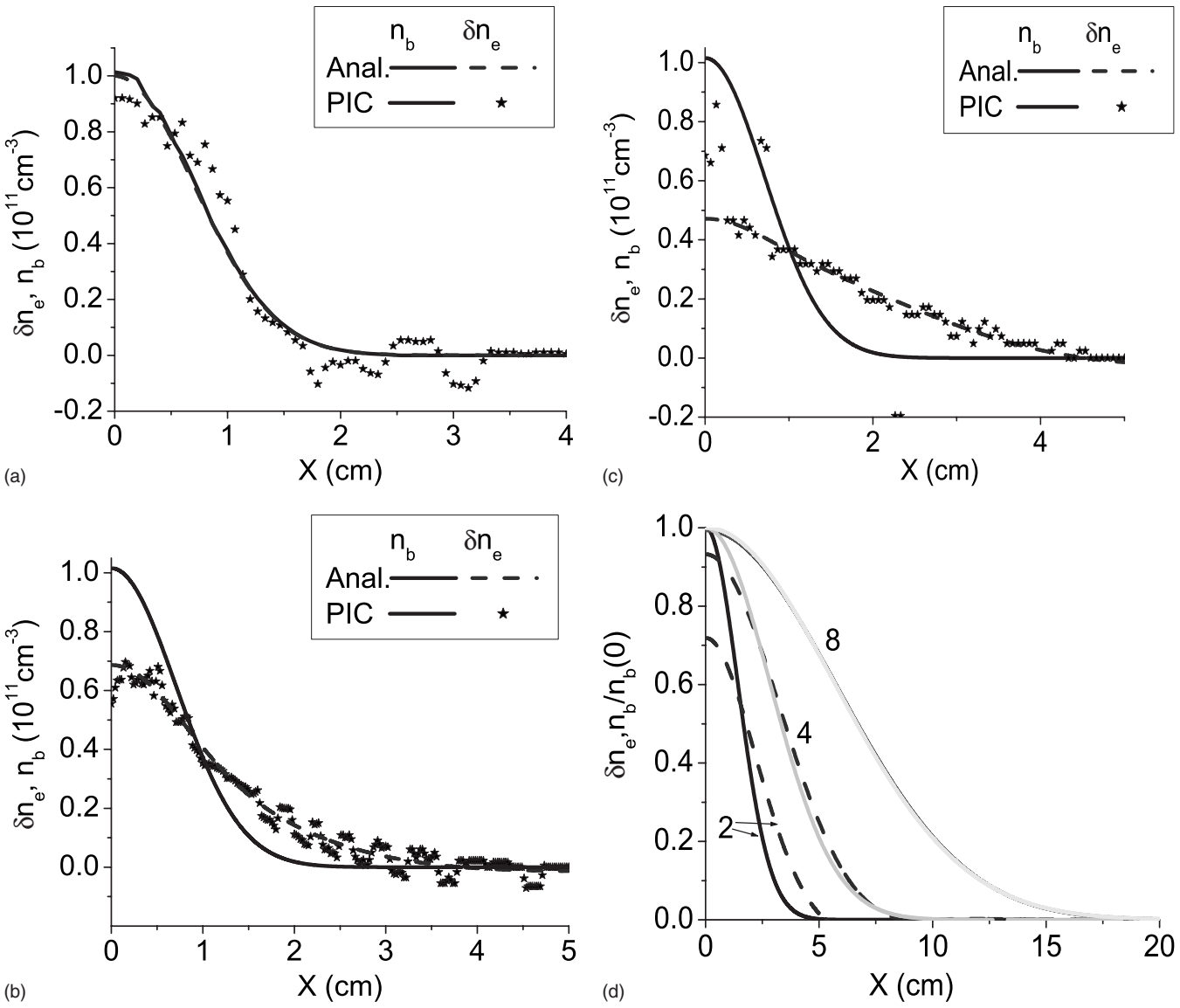

FIG. 8. Comparison of analytic theory and LSP particle-in-cell simulation results for the perturbation in the electron density. The beam velocity is $V_b=0.808c$. The plasma and beam parameters are $n_p=4.8\times10^{11}$ cm^{-3}, $n_{b0}=10^{11}$ cm^{-3}. The beam density profile is Gaussian, $n_{b0}\exp(-r^2/r_b^2)$, where $r_b=1$ cm, except for (d). The values of the applied solenoidal magnetic field, B_{z0}, are: (a) $B_{z0}=0$ G; (b) $B_{z0}=3600$ G; (c) $B_{z0}=5400$ G. (b) shows the effect of the beam radius on the perturbation in the electron density for the parameters in case (c), but with the beam radius equal to 2, 4, and 8 cm; only analytic calculations are shown.

$$E_r=-\frac{Z_b n_{b0}}{n_p\left(1+\frac{\omega_{ce}^2}{\omega_{pe}^2}\right)}\frac{mV_{bz}^2}{e\delta_p}\frac{\omega_{ce}^2}{\omega_{pe}^2\beta_b^2}\left[\frac{\partial a_z}{\partial\rho}+a_\phi\right]. \tag{51}$$

Figure 6(f) and Fig. 7 show the effects of the modification of Eq. (27) to Eq. (46). For the conditions in Fig. 6(f), $\omega_{ce}^2/\omega_{pe}^2=0.33$, and this 30% correction brings the analytic results much closer the PIC simulation results. Figure 7 shows the self-magnetic and self-electric fields for a faster beam pulse than shown in Fig. 6, with $V_b=0.808c$. Figure 7(a) shows the case without any applied magnetic field; the notation "Nonlin. Anal." denotes the results calculated from Eq. (26) where the perturbation in the electron density (nonlinear term) in the return current (n_eA_z, $n_e=n_p+Z_bn_b$) is taken into account; because $n_b/n_p\sim0.1$, this term accounts for about 10% of the difference between the nonlinear and linear theories. Figures 7(b)–7(d) show the results of linear theory when the solenoidal magnetic field is applied. The notation "Full Anal." denotes the results calculated from the system Eqs. (26) and Eq. (46), whereas the notation "Anal." denotes the system of equations corresponding to Eqs. (26) and (27). The difference becomes noticeable for $B=1.8$ kG, where $\omega_{ce}^2/\omega_{pe}^2=0.66$. At the larger value of the magnetic field $B=3.6$ kG, $\omega_{ce}^2/\omega_{pe}^2=2.6$ and the solutions to Eqs. (26) and (27) show the excitation of waves, whereas the system of equations corresponding to Eqs. (26) and (46) does not, as described in Sec. V.

Figure 8 shows the perturbation in the electron density for $B=0,3.6,5.4$ kG, which corresponds to $\omega_{ce}/\omega_{pe}=0,1.6,2.4$. It is evident that for cases (b) and (c) the quasineutrality condition breaks down, which corresponds to $\omega_{ce}>\omega_{pe}$. However, when the beam radius is increased, this

leads to a decrease in the radial electric field according to Eq. (51), and consequently the quasineutrality condition is restored for the perturbation in the electron density as shown in Fig. 8(d).

IV. RADIAL FORCE ACTING ON THE BEAM PARTICLES

The radial force acting on the beam particles is

$$F_r = eZ_b\left(-\frac{1}{c}V_{bz}B_\phi + E_r\right), \tag{52}$$

where the radial electric field is given by Eq. (32). Without the solenoidal magnetic field applied, substituting Eq. (32) into Eq. (52) gives

$$F_r = -\frac{eZ_b}{c}(V_{bz} - V_{ez})B_\phi, \tag{53}$$

and the radial force is always focusing, because the electron flow velocity in the return current is always smaller than the beam velocity, $V_{ez} < V_{bz}$.[20] However, in the presence of the solenoidal magnetic field, the radial force can change sign from focusing to defocusing, because the radial electric field grows faster than the magnetic force $-Z_bV_{bz}B_\phi$, as the solenoidal magnetic field increases. To demonstrate this tendency analytically, let us consider only linear terms in the radial force equation assuming $n_b \ll n_p$. In this limit, the nonlinear terms in Eq. (32) can be neglected, which gives

$$F_r = -\frac{eZ_b}{c}(V_{bz}B_\phi + V_{e\phi}B_z), \tag{54}$$

where $V_{e\phi}$ is given by Eq. (25).

Substituting Eqs. (36) and (37) into Eq. (54) then gives

$$F_r = \frac{Z_b^2 n_{b0}}{n_p}\frac{mV_{bz}^2}{\delta_p}\left[\frac{\partial a_z}{\partial \rho} - \frac{\omega_{ce}^2}{(\omega_{pe}^2+\omega_{ce}^2)\beta_b^2}\left(\frac{\partial a_z}{\partial \rho} + a_\phi\right)\right]. \tag{55}$$

From Eq. (55), it is evident that, in the limit $\omega_{ce}^2 < (\omega_{pe}^2 + \omega_{ce}^2)\beta_b^2$ or $\omega_{ce} < \omega_{pe}\gamma_b\beta_b$ [where $\gamma_b^2 = 1/(1-\beta_b^2)$], the radial force is focusing ($\partial a_z/\partial r < 0$), but if $\omega_{ce} > \omega_{pe}\gamma_b\beta_b$, the radial force can become defocusing. Figure 9 shows the evolution of the radial profile of the normalized radial force for a nonrelativistic beam $\beta_b \ll 1$ [the term in the square bracket on the right-hand side of Eq. (55)] acting on the beam particles for various values of the parameter $\omega_{ce}^2/\omega_{pe}^2\beta_b^2$. The radial force is nearly zero when $\omega_{ce}^2/\omega_{pe}^2\beta_b^2 = 1.5$ for the main part of the beam pulse. This value can be optimal for beam transport over long distances to avoid the pinching effect. Note that the radial force is focusing at larger radius, which can help to minimize halo formation and produce a tighter beam.

Figure 10 shows the optimum value of the parameter $\omega_{ce}^2/\omega_{pe}^2\beta_b^2$, ($\omega_{ce}^2/\omega_{pe}^2\beta_b^2|_{op}$), plotted as a function of r_b/δ_p corresponding to the minimum radial force for effective beam transport over long distances. Note that for small r_b/δ_p, $\omega_{ce}^2/\omega_{pe}^2\beta_b^2|_{op}$ is approximately equal to unity, and increases with r_b/δ_p to the limiting value 4; this value corresponds to the onset of excitation of whistler and lower-hybrid-like waves. For $\omega_{ce}^2/\omega_{pe}^2\beta_b^2 > 4$ the structure of the self-electromagnetic field becomes rather complicated,[37] and the transport of very intense beam pulses with $r_b/\delta_p > 6$ in the presence of a solenoidal magnetic field can be strongly affected by collective wave generation, as discussed in the next section.

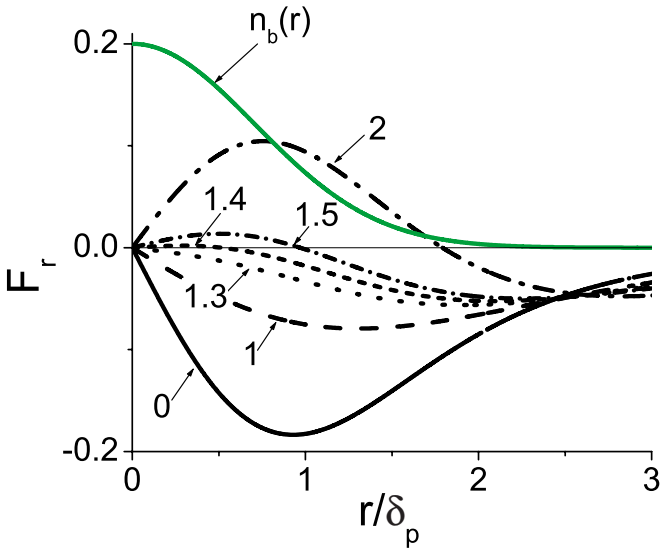

FIG. 9. (Color online) The normalized radial force $F_r/(Z_b^2 n_{b0} m V_{bz}^2/n_p\delta_p)$ acting on the beam particles for different values of the parameter $\omega_{ce}^2/\omega_{pe}^2\beta_b^2$. The gray line (green online) shows the Gaussian density profile multiplied by 0.2 in order to fit the profile into the plot. The beam radius is equal to the skin depth, $r_b = \delta_p$.

V. BEAM EXCITATION OF THE WHISTLER AND HELICON WAVES

In this section, we explicitly take into account that the beam can be relativistic. As shown below, excitation of the waves disappears in the limit of a relativistic beam with $\gamma_b \gg 1$. In the case of a dense background plasma, $n_p \gg n_b$, the electron velocity is much smaller than the speed of light; and

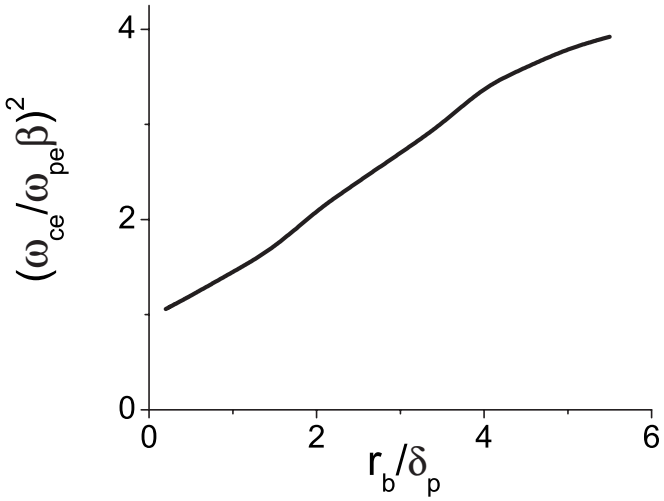

FIG. 10. The parameter $\omega_{ce}^2/\omega_{pe}^2\beta_b^2|_{op}$ plotted as a function of r_b/δ_p corresponding to the minimum radial force for effective beam transport over long distances. The beams have Gaussian density profiles with different values of r_b/δ_p.

relativistic corrections to the electron motion need not be taken into account.[20] Equations (26) and (46) support wave excitations when

$$\frac{\omega_{ce}}{\omega_{pe}} > 2\beta_b\gamma_b^2. \tag{56}$$

Indeed, looking for solutions of Eqs. (26) and (46) proportional to $\exp(ikx)$ for a uniform plasma in the absence of a beam pulse, some straightforward algebra gives

$$\beta_b^2\left(1+\frac{1}{\varpi^2}\right)k^4\delta_p^4+\left[\beta_b^2\left(1+\frac{1}{\varpi^2}\right)+\frac{\beta_b^2}{\varpi^2}-1\right]k^2\delta_p^2+\frac{\beta_b^2}{\varpi^2}=0, \tag{57}$$

where $\varpi=\omega_{ce}/\omega_{pe}$. Equation (57) can be also derived from the general dispersion relation for electromagnetic waves (see for example, Refs. 38 and 39),

$$A\left(\frac{kc}{\omega}\right)^4+B\left(\frac{kc}{\omega}\right)^2+C=0, \tag{58}$$

where $A=\varepsilon_\perp\sin^2\theta+\varepsilon_\parallel\cos^2\theta$, $B=-\varepsilon_\perp\varepsilon_\parallel(1+\cos^2\theta)-(\varepsilon_\perp^2-g^2)\sin^2\theta$, $C=\varepsilon_\parallel(\varepsilon_\perp^2-g^2)$. In the dispersion relation (58), $\varepsilon_\perp,\varepsilon_\parallel,g$ are components of the plasma dielectric tensor, $\cos\theta=k_\parallel/k$ is the angle of wave propagation relative to the magnetic field, $k_\parallel$ is the $k_\parallel$-vector along the direction of the solenoidal magnetic field, and $k=|\mathbf{k}|$. Here, we account for the fact that for long beam pulses, only waves with $k_\parallel$-vectors nearly perpendicular to the beam velocity are excited, $k_\parallel \ll k_\perp \simeq k$. The wave phase-velocity should coincide with the beam velocity for a steady-state wave pattern in the beam frame, i.e.,

$$\omega = V_b k_\parallel. \tag{59}$$

When small terms of order $k_\parallel^2\delta_p^2$ and $k_\parallel^2\delta_p^2/\varpi^2$ are neglected in the general dispersion relation, Eq. (58), the resulting equation becomes Eq. (57). The solution to Eq. (57) is

$$k^2\delta_p^2=\frac{\varpi^2-2\beta_b^2\gamma_b^2\pm\sqrt{\varpi^2(\varpi^2-4\beta_b^2\gamma_b^4)}}{2\beta_b^2\gamma_b^2(1+\varpi^2)}. \tag{60}$$

Therefore, when the condition in Eq. (56) is satisfied, waves are excited. Note that the solutions to the approximate system, Eqs. (26) and (27), without taking into account the term corresponding to quasineutrality breaking down (the term proportional to $\omega_{ce}^2/\omega_{pe}^2$ on the left-hand side of the equation for A_ϕ), show the excitation of waves when $\omega_{ce}/\omega_{pe}>2\beta_b$. The difference between this approximate condition and the exact condition given by Eq. (56) is sizable when $\beta_b\to 1$. For example, for the conditions in Fig. 7, $\beta_b=0.808$ and for the conditions in Fig. 7(d), $\omega_{ce}/\omega_{pe}=1.621>2\beta_b=1.617$, and waves are not excited, whereas the approximate criterion predicts excitation of waves. Particle-in-cell simulation results show that waves are not excited even for twice larger values of the magnetic field because the critical value of ω_{ce}/ω_{pe} is equal to $2\beta_b\gamma_b^2=4.7$, which justifies the criterion given in Eq. (56).

A. Excitation of helicon (lower-hybrid-like) waves

In the limit $\varpi\gg 2\beta_b\gamma_b^2$, the upper-root solution in Eq. (60) tends to $k\delta_p=\varpi/\beta_b\gamma_b(1+\varpi^2)^{1/2}$, and substituting the definition of ϖ gives

$$k\to k_+=k_{\mathrm{lh}}=\frac{\omega_{ce}\omega_{pe}}{c\beta_b\gamma_b(\omega_{ce}^2+\omega_{pe}^2)^{1/2}}. \tag{61}$$

This mode corresponds to the excitation of helicon (lower-hybrid-like) waves. Consider nonrelativistic beam pulses with $\beta_b\ll 1$, then the lower-hybrid frequency is[38,39]

$$\omega=\frac{\omega_{ce}\omega_{pe}}{(\omega_{ce}^2+\omega_{pe}^2)^{1/2}}\cos\theta. \tag{62}$$

Figure 11 shows the excitation of helicon (lower-hybrid-like) waves observed in simulations using the LSP particle-in-cell code.

Substituting Eq. (59) into Eq. (62) and using $\cos\theta=k_\parallel/k$, yields the limiting value $k\to k_+$ for lower-hybrid waves given by Eq. (61). As evident from Eq. (60), for $\varpi>2\beta_b$, $k_{\mathrm{lh}}\delta_p>1$ and the lower-hybrid waves have short wavelengths, of order or smaller than the skin depth in agreement with PIC simulation results.[29] Lower-hybrid waves were observed in PIC simulations.[27,29] Note that for relativistic beams there is an extra factor $1/\gamma_b$ in Eq. (61) compared with the derivation based on the lower hybrid frequency, Eq. (62). This is because the traditional analysis for the plasma resonances (including the lower hybrid frequency) assumes $A=0$, whereas a more rigorous calculation shows that in the limit $\cos\theta\to 0$ the second term with the B factor has also to be taken into account when solving Eq. (58). Due to this subtle difference we call these waves "lower-hybrid-like" waves not simply lower-hybrid waves. Similar to the low-hybrid waves if $\cos\theta=k_\parallel/k\tilde{}r_b/l_b<(m/M)^{1/2}$ the ion dynamics has to be accounted for.[39] Therefore, this theory is valid for not very long beam pulses $l_b<r_b(M/m)^{1/2}$.

In addition to a steady-state pattern of waves in the beam frame,[27] nonstationary lower-hybrid waves were observed propagating perpendicular to a strong solenoidal magnetic field when the beam parameters changes rapidly near the focal plane.[29] A similar excitation of helicon waves during fast penetration of the magnetic field due to the Hall effect in high energy plasma devices, such as plasma opening switches and Z pinches, was observed in Refs. 30. Coupling of the helicon waves to the plasma or the beam ions can lead to development of the electrostatic modified two-stream instability.[44]

B. Excitation of whistler waves

The lower-root solution in Eq. (60) in the limit $\varpi\gg 2\beta_b\gamma_b^2$ tends to $k\delta_p=\beta_b\gamma_b/\varpi$ and describes long wavelength perturbations. Substituting the definition of ϖ gives

$$k\to k_-=k_{\mathrm{wh}}=\frac{\omega_{pe}^2\beta_b\gamma_b}{c\omega_{ce}}, \tag{63}$$

corresponding to whistler-wave excitation. Excitation of whistler waves in cylindrical geometry can be derived from Eq. (34) directly by assuming that the wavelength is large

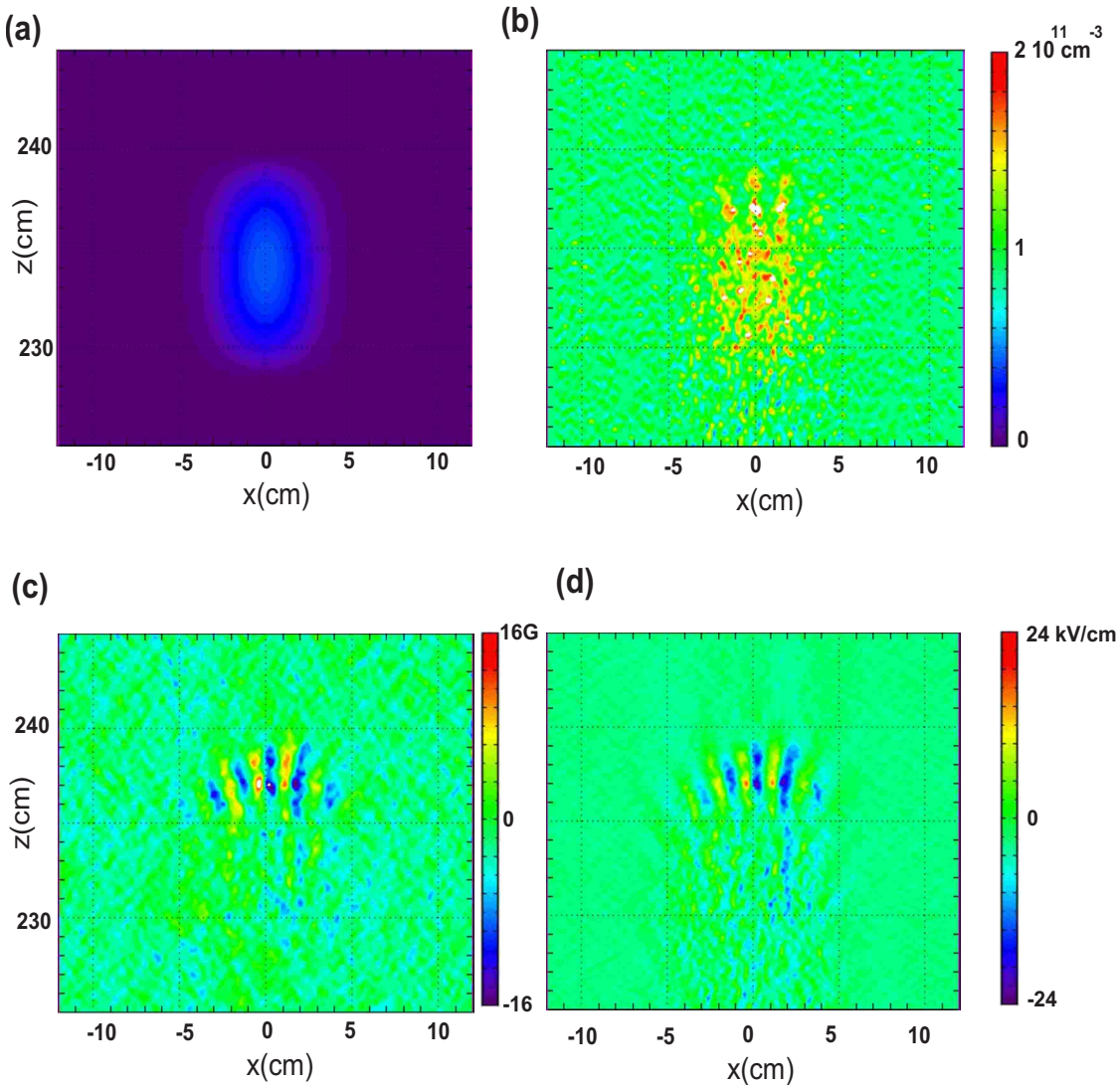

FIG. 11. (Color online) LSP particle-in-cell simulation results for the perturbations in electron density, self-magnetic field, and self-electric radial field. The beam velocity is $V_b=0.2c$. The plasma and beam parameters are $n_p=10^{11}$ cm^{-3}, and $n_{b0}=0.5\times10^{11}$ cm^{-3}. The beam density profile is Gaussian, $n_{b0}\exp(-z^2/l_b^2-r^2/r_b^2)$, where $r_b=2.8$ cm, and $l_b=5.7$ cm. The value of the applied solenoidal magnetic field is $B_{z0}=2839$ G. (a) shows the beam density; (b) the electron density; (c) the self-magnetic field B_y; and (d) the self-electric field E_x.

compared with the skin depth $k_{ws}\delta_p \ll 1$. Then the terms on the left-hand side of Eqs. (26) and (27) can be neglected, and neglecting the small ion beam rotation gives

$$\frac{e}{mc}n_e A_\phi = -\frac{B_z}{4\pi m V_b}\frac{\partial A_z}{\partial r}. \tag{64}$$

Substituting Eq. (64) into Eq. (26) yields

$$\frac{cB_z^2}{(4\pi)^2 emn_e V_b^2}\frac{1}{r}\frac{\partial}{\partial r}\left(r\frac{\partial A_z}{\partial r}\right)+\frac{e}{mc}n_e A_z = Z_b n_b V_{bz}. \tag{65}$$

Equation (65) describes oscillations with wavelength

$$\lambda_{\mathrm{wh}} = \frac{cB_z}{2en_p V_b}, \tag{66}$$

which correspond to whistler waves.[18] Indeed, the dispersion relation for whistler waves is[39]

$$\omega^2 = \frac{\omega_{ce}^2 c^2}{\omega_{pe}^4}\left(k_\parallel^2+\frac{\omega_{pi}^2}{c^2}\right)k^2,$$

where ω_{pi} is the ion plasma frequency and $k_\parallel$ is the wavenumber along the magnetic field. Assuming that the beam pulse length is not very long, i.e., $k_\parallel \sim 1/l_b \gtrsim \omega_{pi}/c$, the whistler wave dispersion relation becomes

$$\omega = \frac{\omega_{ce}c}{\omega_{pe}^2}k_\parallel k. \tag{67}$$

Because the perturbations correspond to a steady-state wave pattern in the beam frame, $\omega=V_b k_\parallel$ in the laboratory frame. Substituting Eq. (59) into Eq. (67) shows that the whistler waves are excited with the same wavenumber perpendicular to the beam velocity[18]

$$k_{\mathrm{wh}} = \frac{\omega_{pe}^2 V_b}{\omega_{ce} c},$$

which is equivalent to Eq. (63) or Eq. (66).

Particle-in-cell simulations show that structure of the self-electric and self-magnetic fields excited by the beam in the presence of whistler and lower-hybrid waves becomes rather complex,[27,29] and will be discussed in future publications. Coupling of helicon waves to the beam ion oscillations can lead to the development of the modified two-stream instability.[44]

VI. CONCLUSIONS

Application of a solenoidal magnetic field strongly affects the degree of current and charge neutralization when

$$\frac{\omega_{ce}}{\omega_{pe}} > \gamma_b \beta_b, \tag{68}$$

$(\gamma_b = 1/\sqrt{1-\beta_b^2})$ or equivalently,

$$B > 320 \gamma_b \beta_b \sqrt{\frac{n_p[\mathrm{cm}^{-3}]}{10^{10}}}\ \mathrm{G}. \tag{69}$$

The threshold value of B given in Eq. (69) corresponds to relatively small values of the magnetic field for nonrelativistic beams. When the criterion in Eq. (69) is satisfied, application of the solenoidal magnetic field leads to three unexpected effects:

(1) The first effect is the dynamo effect, in which the electron rotation generates a self-magnetic field that is much larger than in the limit with no applied magnetic field.
(2) The second effect is the generation of a large radial electric field. Because the $v_\phi \times B_z$ force should be balanced by a radial electric field, the spinning results in a plasma polarization and produces a much larger self-electric field than in the limit with no applied field.
(3) The third unexpected effect is that the joint system consisting of the ion beam pulse and the background plasma act as a paramagnetic medium, i.e., the solenoidal magnetic field is enhanced inside of the ion beam pulse.

Application of the solenoidal magnetic field can be used for active control of beam transport through background plasma. Without the applied solenoidal magnetic field, the radial force is always focusing, because the magnetic attraction of parallel currents in the beam always dominates the radial electric field, which is screened by the plasma better than the self-magnetic field. However, when a solenoidal magnetic field is applied, the radial electric force can become larger than the magnetic force, resulting in beam defocusing. Figure 10 shows the optimum value of the parameter $\omega_{ce}^2/\omega_{pe}^2\beta_b^2|_{op}$ plotted as a function of the ratio of the beam radius to the skin depth, r_b/δ_p, corresponding to the minimum radial force for effective beam transport over long distances.

For larger values of the solenoidal magnetic field, corresponding to

$$\frac{\omega_{ce}}{\omega_{pe}} > 2\gamma_b^2 \beta_b, \tag{70}$$

or equivalently,

$$B > 640 \gamma_b^2 \beta_b \sqrt{\frac{n_p[\mathrm{cm}^{-3}]}{10^{10}}}\ \mathrm{G}, \tag{71}$$

the beam generates whistler and lower-hybrid waves. For nonrelativistic beams $\beta_b \ll 1$, the whistler waves have long wavelength compared with the skin depth

$$\lambda_{\mathrm{wh}} = \frac{cB_z}{2en_pV_b}, \tag{72}$$

whereas helicon (lower-hybrid-like) waves have short wavelength compared with the skin depth

$$\lambda_w = \frac{2\pi V_b(\omega_{ce}^2 + \omega_{pe}^2)^{1/2}}{\omega_{ce}\omega_{pe}}. \tag{73}$$

When collective waves are excited, the particle-in-cell simulations show that the structure of the self-electromagnetic field becomes rather complex, and the transport of very intense beam pulses can be strongly affected by the wave generation,[27,29] which will be discussed in future publications.

Beam propagation in a plasma is considered to be an effective way to compress intense beam pulses both longitudinally and transversely by applying a small velocity tilt.[8,17] A number of possible instabilities during propagation of beam pulses through a background plasma in a solenoidal magnetic field[40,41] can be effectively mitigated by a small velocity tilt and plasma density inhomogeneity.[42,43]

In a follow-up publication the limit of strong magnetic field will be discussed.[33]

ACKNOWLEDGMENTS

We thank Mikhail Dorf, Bryan Oliver, Dale Welch, Jean-Luc Vay, and Alex Friedman for fruitful discussions.

This research was supported by the U.S. Department of Energy Office of Fusion Energy Sciences and the Office of High Energy Physics.

[1] H. Alfven, Phys. Rev. **55**, 425 (1939).
[2] W. H. Bennett, Phys. Rev. **45**, 890 (1934).
[3] M. V. Medvedev and A. Loeb, Astrophys. J. **526**, 697 (1999); M. V. Medvedev, M. Fiore, R. A. Fonseca, L. O. Silva, and W. B. Mori, Astrophys. J. Lett. **618**, L75 (2005); A. Gruzinov, *ibid.* **563**, L15 (2001); A. Spitkovsky, *ibid.* **673**, L39 (2008).
[4] A. R. Bell, Mon. Not. R. Astron. Soc. **358**, 181 (2005).
[5] P. Chen, J. M. Dawson, R. W. Huff, and T. Katsouleas, Phys. Rev. Lett. **54**, 693 (1985).
[6] R. Govil, W. P. Leemans, E. Yu. Backhaus, and J. S. Wurtele, Phys. Rev. Lett. **83**, 3202 (1999); G. Hairapetian, P. Davis, C. E. Clayton, C. Joshi, S. C. Hartman, C. Pellegrini, and T. Katsouleas, *ibid.* **72**, 2403 (1994).
[7] M. Roth, T. E. Cowan, M. H. Key, S. P. Hatchett, A. Snavely, S. C. Wilks, K. Yasuike, H. Ruhl, F. Pegoraro, S. V. Bulanov, E. M. Campbell, M. D. Perry, and H. Powell, Phys. Rev. Lett. **86**, 436 (2001); M. Tabak, J. Hammer, M. E. Glinsky, W. L. Kruer, S. C. Wilks, J. Woodworth, E. M. Campbell, M. D. Perry, and R. J. Mason, Phys. Plasmas **1**, 1626 (1994). R. B. Campbell, R. Kodama, T. A. Mehlhorn, K. A. Tanaka, and D. R. Welch, Phys. Rev. Lett. **94**, 055001 (2005); Y. Sentoku, K. Mima, P. Kaw, and K. Nishikawa, *ibid.* **90**, 155001 (2003); T. Taguchi, T. M. Antonsen, Jr., C. S. Liu, and K. Mima, *ibid.* **86**, 5055 (2001); A. J. Kemp, Y.

Sentoku, V. Sotnikov, and S. C. Wilks, *ibid.* **97**, 235001 (2006); R. J. Mason, *ibid.* **96**, 035001 (2006).
[8]P. K. Roy, S. S. Yu, and E. Henestroza, Phys. Rev. Lett. **95**, 234801 (2005); E. Henestroza, A. Anders, F. M. Bieniosek, W. G. Greenway, B. G. Logan, W. L. Waldron, D. L. Vanecek, D. R. Welch, D. V. Rose, R. C. Davidson, P. C. Efthimion, E. P. Gilson, A. B. Sefkow, and W. M. Sharp, Phys. Plasmas **11**, 2890 (2004); Nucl. Instrum. Methods Phys. Res. A **544**, 225 (2005).
[9]M. Anderson, M. Binderbauer, V. Bystritskii, E. Garate, N. Rostoker, Y. Song, A. Van Drie, and I. Isakov, Plasma Phys. Rep. **31**, 809 (2005); V. Bystritskii, E. Garate, N. Rostoker, Y. Song, A. Vandrie, and M. Anderson, J. Appl. Phys. **96**, 1249 (2004); H. Yamada, H. Ji, S. Gerhardt, E. V. Belova, R. C. Davidson, and D. R. Mikkelsen, J. Plasma Fusion Res. **2**, 004 (2007); H. Ji, E. Belova, S. P. Gerhardt, and M. Yamada, J. Fusion Energy **26**, 93 (2007).
[10]T. N. Larosa and A. Gordon, Sol. Phys. **120**, 343 (1989).
[11]M. D. Gabovich, Sov. Phys. Usp. **20**, 134 (1977); I. A. Soloshenko, Rev. Sci. Instrum. **67**, 1646 (1996).
[12]W. M. Sharp, D. A. Cahallan, and M. Tabak, Fusion Sci. Technol. **43**, 393 (2003); D. Callahan, Fusion Eng. Des. **32–33**, 441 (1996); D. R. Welch, D. V. Rose, W. M. Sharp, C. L. Olson, and S. S. Yu, Laser Part. Beams **20**, 621 (2002); Nucl. Instrum. Methods Phys. Res. A **544**, 236 (2005).
[13]I. D. Kaganovich, E. Startsev, and R. C. Davidson, Phys. Plasmas **11**, 3546 (2004).
[14]W. M. Sharp, D. A. Callahan, M. Tabak, S. S. Yu, P. F. Peterson, D. V. Rose, and D. R. Welch, Fusion Sci. Technol. **44**, S221 (2004).
[15]C. Burkhart and S. Humphries, Jr., *Proceedings of the 12th IEEE Particle Accelerator Conference*, 16–19 March 1987, Washington, D.C., p. 1037; http://accelconf.web.cern.ch/AccelConf/p87/PDF/PAC1987_1037.PDF.
[16]A. F. Lifschitz, G. Maynard, and J. L. Vay, Nucl. Instrum. Methods Phys. Res. A **544**, 202 (2005); A. F. Lifschitz, G. Maynard, J. L. Vay, and A. Lenglet, J. Phys. IV **133**, 754 (2006); J.-L. Vay and C. Deutsch, Nucl. Instrum. Methods Phys. Res. A **464**, 293 (2001); Phys. Plasmas **5**, 1190 (1998).
[17]C. M. Celata, F. M. Bieniosek, E. Henestroza, J. W. Kwan, E. P. Lee, G. Logan, L. Prost, P. A. Seidl, J. L. Vay, W. L. Waldron, S. S. Yu, J. J. Barnard, D. A. Callahan, R. H. Cohen, A. Friedman, D. P. Grote, S. M. Lund, A. Molvik, W. M. Sharp, G. Westenskow, R. C. Davidson, P. Efthimion, E. Gilson, L. R. Grisham, I. Kaganovich, H. Qin, E. A. Startsev, S. Bernal, Y. Cui, D. Feldman, T. F. Godlove, I. Haber, J. Harris, R. A. Kishek, H. Li, P. G. O'Shea, B. Quinn, M. Reiser, A. Valfells, M. Walter, Y. Zou, D. V. Rose, and D. R. Welch, Phys. Plasmas **10**, 2063 (2003); B. G. Logan, F. M. Bieniosek, C. M. Celata, E. Henestroza, J. W. Kwan, E. P. Lee, M. Leitner, P. K. Roy, P. A. Seidl, S. Eylon, J.-L. Vay, W. L. Waldron, S. S. Yu, J. J. Barnard, D. A. Callahan, R. H. Cohen, A. Friedman, D. P. Grote, M. Kireeff Covo, W. R. Meier, A. W. Molvik, S. M. Lund, R. C. Davidson, P. C. Efthimion, E. P. Gislon, L. R. Grisham, I. D. Kaganovich, H. Qin, E. A. Startsev, D. V. Rose, D. R. Welch, C. L. Olson, R. A. Kishek, P. O'Shea, I. Haber, and L. R. Prost, Nucl. Instrum. Methods Phys. Res. A **577**, 1 (2007).
[18]B. V. Oliver, D. D. Ryutov, and R. N. Sudan, Phys. Plasmas **1**, 3383 (1994).
[19]B. V. Oliver, D. D. Ryutov, and R. N. Sudan, Phys. Plasmas **3**, 4725 (1996).
[20]I. D. Kaganovich, G. Shvets, E. A. Startsev, and R. C. Davidson, Phys. Plasmas **8**, 4180 (2001).
[21]I. D. Kaganovich, E. A. Startsev, A. B. Sefkow, and R. C. Davidson, Phys. Rev. Lett. **99**, 235002 (2007).
[22]O. Polomarov, A. B. Sefkow, I. D. Kaganovich, and G. Shvets, Phys. Plasmas **14**, 043103 (2007).
[23]I. D. Kaganovich, E. Startsev, and R. C. Davidson, Laser Part. Beams **20**, 497 (2002).
[24]I. D. Kaganovich, E. Startsev, and R. C. Davidson, Phys. Scr., T **107**, 54 (2004).
[25]I. D. Kaganovich, E. Startsev, and R. C. Davidson, Nucl. Instrum. Methods Phys. Res. A **544**, 383 (2005).
[26]R. N. Sudan and P. M. Lyster, Comments Plasma Phys. Controlled Fusion **9**, 453 (1984); D. W. Hewett, Nucl. Fusion **24**, 349 (1984).
[27]I. D. Kaganovich, A. B. Sefkow, E. A. Startsev, R. C. Davidson, and D. R. Welch, Nucl. Instrum. Methods Phys. Res. A **577**, 93 (2007).
[28]J. S. Pennington, I. D. Kaganovich, E. A. Startsev, A. B. Sefkow, and R. C. Davidson, Particle Accelerator Conference, 365 (2007), http://cern.ch/AccelConf/p07/PAPERS/THPAS083.PDF.
[29]A. B. Sefkow, R. C. Davidson, I. D. Kaganovich, E. P. Gilson, P. K. Roy, S. S. Yu, P. A. Seidl, D. R. Welch, D. V. Rose, and J. J. Barnard, Nucl. Instrum. Methods Phys. Res. A **577**, 289 (2007); Ph.D. thesis, Princeton University, 2007.
[30]M. B. Isichenko and A. M. Marnachev, Sov. Phys. JETP **66**, 702 (1987); Ya. L. Kalda and A. S. Kingsep, Sov. J. Plasma Phys. **15**, 508 (1989); Ja. Kalda, Phys. Rev. E **54**, 1824 (1996).
[31]H. L. Berk and L. D. Pearlstein, Phys. Fluids **19**, 1831 (1976); K. R. Chu and N. Rostoker, *ibid.* **16**, 1472 (1973); R. Lee and R. N. Sudan, *ibid.* **14**, 1213 (1971). S. E. Rosinskii and V. G. Rukhlin, Sov. Phys. JETP **37**, 436 (1973).
[32]V. I. Pistunovich, V. V. Platonov, V. D. Ryutov, and E. A. Filimonova, Sov. J. Plasma Phys. **2**, 418 (1976).
[33]I. D. Kaganovich, E. A. Startsev, M. Dorf, and R. C. Davidson, "Controlling charge and current neutralization of an ion beam pulse in a background plasma by application of a solenoidal magnetic field: Strong magnetic field limit," Phys. Plasmas (unpublished).
[34]O. Buneman, Proc. R. Soc. London, Ser. A **215**, 346 (1952).
[35]L. D. Landau and E. M. Lifshitz, *Electrodynamics of Continuous Media* (Pergamon, Oxford, 1993).
[36]T. P. Hughes, S. S. Yu, and R. E. Clark, Phys. Rev. ST Accel. Beams **2**, 110401 (1999); D. R. Welch, D. V. Rose, B. V. Oliver, T. C. Genoni, R. E. Clark, C. L. Olson, and S. S. Yu, Phys. Plasmas **9**, 2344 (2002).
[37]M. Dorf, I. D. Kaganovich, E. A. Startsev, and R. C. Davidson, "Self-focusing on an ion beam propagating through a background neutralizing plasma along a solenoidal magnetic field," Phys. Plasmas (unpublished).
[38]A. I. Akhiezer, I. A. Akhiezer, R. V. Polovin, A. G. Sitenko, and K. N. Stepanov, *Plasma Electrodynamics* (Nauka, Moscow, 1974).
[39]E. M. Lifshitz and L. P. Pitaevskii, *Physical Kinetics* (Pergamon, Oxford, 1981).
[40]R. J. Briggs, *Electron Stream Interaction With Plasmas* (MIT, Cambridge, 1964).
[41]V. B. Krasovitskii, *Instabilities of a Relativistic Electron Beam in Plasma* (Nova Science, New York, 2007).
[42]C. Thoma, D. R. Welch, S. S. Yu, E. Henestroza, P. K. Roy, S. Eylon, and E. P. Gilson, Phys. Plasmas **12**, 043102 (2005).
[43]E. A. Startsev and R. C. Davidson, Nucl. Instrum. Methods Phys. Res. A **577**, 79 (2007).
[44]E. A. Startsev, R. C. Davidson, and M. Dorf, Phys. Plasmas **15**, 062107 (2008).